

1 **Cobalt-60, Barium-133, Cesium-137, and Europium-152 migration from cementitious sources through**
2 **sediment under field conditions**

3 Reid Williams(1)*, Daniel I. Kaplan(2), Bryan J. Erdmann(3), Timothy A. DeVol(1,4), and Brian A.
4 Powell(1,4)*

5 (1) Department of Environmental Engineering and Earth Sciences, Clemson University, 342 Computer
6 Court, Anderson, SC, 29625, USA.

7 (2) Savannah River Ecology Laboratory, University of Georgia, Aiken, SC 29802, USA

8 (3) Environmental Restoration Group, Albuquerque, NM, 87113, USA

9 (4) Center for Nuclear Environmental Engineering Sciences and Radioactive Waste Management Center
10 (NEESRWM), Clemson University, Clemson, SC, 29634, USA

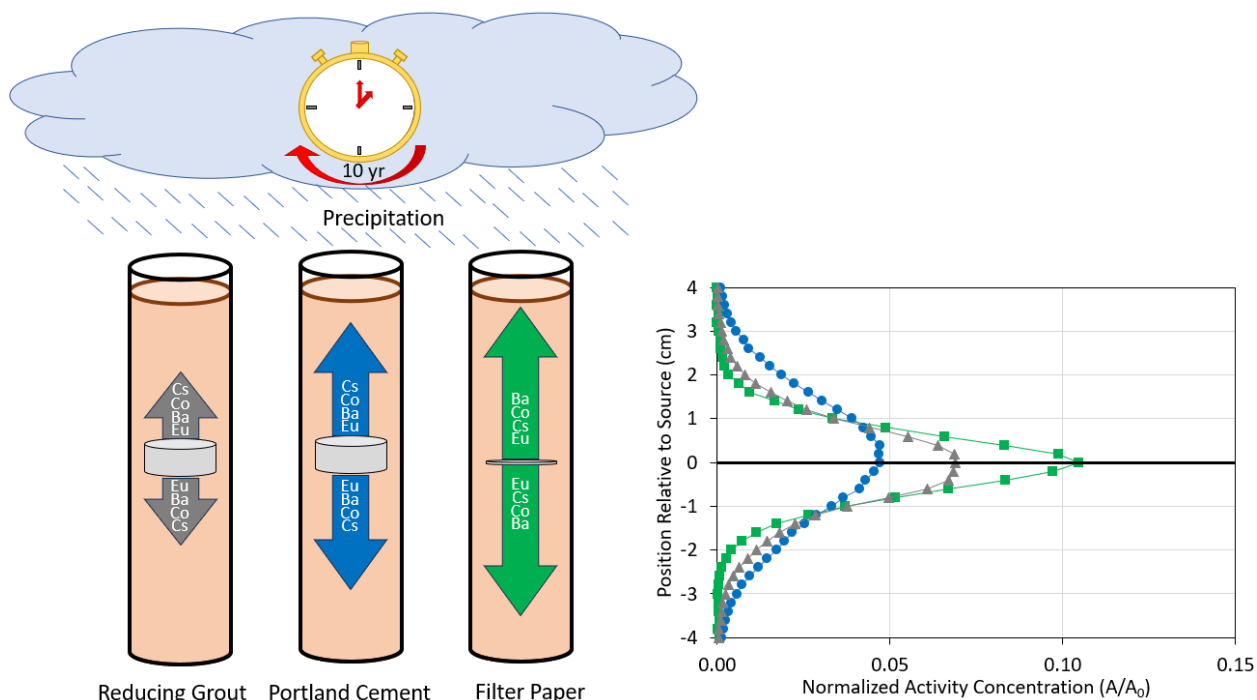
11 *Corresponding Authors: r fw@clemson.edu, bpowell@clemson.edu, (864) 656-1004

12

13 **Keywords:** Lysimeter, vadose zone, non-destructive gamma-ray spectroscopy, Portland cement, reducing
14 grout

15 **Abstract**

16 Safe and effective storage of radioactive waste is essential to protect human and environmental
17 health. Due to the potential for accidental releases and the severity of the associated risks, it is
18 imperative to further understand radionuclide transport should an accident occur. This study was the
19 second set of measurements conducted in 2022 of an ongoing experiment that has analyzed the vadose
20 zone migration of radionuclides from cementitious wastefoms at the Savannah River Site over the last
21 ten years. The radionuclides introduced within the sources are prominent constituents of radioactive
22 waste or analogs for other groups or series of radionuclides. Lysimeters were first analyzed in 2016 using
23 a collimated high-purity germanium gamma-ray spectrometer to non-destructively measure the
24 concentration of each radionuclide in the sediment column as a function of depth. Following these
25 measurements, the lysimeters were redeployed for another 4 years. All radionuclides in all lysimeters
26 were observed to transport further during the redeployment period; however, the extent of migration
27 varied with the material used for introduction. Except for ^{137}Cs , migration through the sediment control
28 system increased with decreasing ionic potential (ionic charge/radius); migration order:
29 $^{152}\text{Eu} < ^{137}\text{Cs} < ^{60}\text{Co} < ^{133}\text{Ba}$. Overall, the cementitious wastefoms were observed to decrease radionuclide
30 migration extent relative to natural vadose zone conditions. In both cementitious wastefoms, the
31 migration extent increased in the order $^{152}\text{Eu} < ^{133}\text{Ba} < ^{60}\text{Co} < ^{137}\text{Cs}$. However, less migration was measured
32 when the radionuclides were incorporated into a reducing grout wastefom. The novelty of this paper is
33 the demonstration of a technique capable of creating non-destructive measurements over decade time
34 scales. Ultimately, this work provides insight into the long-term migration of alkali, alkali earth, divalent
35 transition metal, and trivalent (*e.g.*, lanthanide and actinide element) isotopes.

36 **Graphical Abstract**

37

38 **1. Introduction**

39 The United States Department of Energy Savannah River Site (SRS) currently contains approximately
 40 100 million liters of radioactive waste in 51 underground storage tanks. Most of the waste in these tanks
 41 is in the soluble salt form and ongoing treatment solidifies the waste into a reducing grout (Kaplan et al.,
 42 2008). This treatment is intended to safely immobilize radioactive liquid waste stored at SRS in solid
 43 forms for permanent on-site disposal. Concurrently, to provide data relevant to site performance
 44 assessment models, the SRS has transport experiments underway at the Radionuclide Field Lysimeter
 45 Experiment (RadFLEX) facility (Roberts et al., 2012). Of interest to this work are the RadFLEX lysimeters
 46 that contain Portland cement (a cementitious material comprised of 45% fly ash, 55% cement), reducing
 47 grout (a cementitious material comprised of 45% fly ash, 45% blast furnace slag, and 10% cement), or
 48 glass filter paper sources (to function as a sediment control) amended with a suite of gamma-emitting
 49 radionuclides to provide information that can be used to estimate risk associated with radioactive waste
 50 disposal (Roberts et al., 2012). In a previous study, Erdmann et al. (Erdmann et al., 2018) used a non-
 51 destructive technique to measure the vertical profiles of four gamma-emitting radioisotopes (⁶⁰Co, ¹³³Ba,
 52 ¹³⁷Cs, ¹⁵²Eu) in lysimeters after four years of deployment in RadFLEX. After the analysis, the lysimeters
 53 were redeployed for continued exposure to environmental conditions. The current work analyzed the
 54 same lysimeters using the same non-destructive approach after an additional 4 years of deployment to
 55 quantify the migration extent of the radionuclides in the lysimeter sediment columns.

56 Gamma-emitting radionuclides ⁶⁰Co, ¹³³Ba, ¹³⁷Cs, and ¹⁵²Eu were selected due to the ability to
 57 measure all four simultaneously using non-destructive gamma-ray spectroscopy and because they are, or
 58 are good analogs for, radioisotopes that are prevalent in radioactive waste. Cesium and barium are
 59 alkaline and alkaline earth metals and will exist in the (I) and (II) oxidation states, respectively. ¹³⁷Cs has a
 60 high fission yield while ¹³³Ba is chemically comparable to ⁹⁰Sr, an alkaline earth element with a high

61 fission yield. Cobalt is a transition metal, and ^{60}Co is an abundant activation product that persists as
62 Co(II) in the SRS vadose zone. Europium is anticipated to exist in the (III) oxidation state in most natural
63 environments, including the SRS vadose zone. Eu(III) was selected for these experiments to provide a
64 relatively strongly sorbing radionuclide species for comparison with the generally more mobile and
65 soluble mono and divalent ions. Furthermore, Eu(III) is commonly used as an analog for trivalent
66 actinides and lanthanides (*e.g.*, $^{241}\text{Am(III)}$ and $^{244}\text{Cm(III)}$) which have been observed in the SRS subsurface
67 (Buesseler et al., 2009) because the stable oxidation state and similar ionic radius yield similar physical
68 and chemical behaviors (Estes et al., 2013; Goo et al., 2021).

69 The mobility of radionuclides through the vadose zone depends on interactions with solid
70 surfaces. SRS sediments are composed primarily of kaolinite and sand and possess a relatively low cation
71 exchange capacity (Table S2). Clay minerals are primarily responsible for cation sorption in SRS sediments
72 (Goto et al., 2008). The clay fraction is composed primarily of kaolinite and hydroxy-interlayered
73 vermiculite (HIV), the product of highly weathered phyllosilicates (Goto et al., 2014, 2008; Naumann et
74 al., 2012; Zaunbrecher et al., 2015). Kaolinite exhibits the lowest cation exchange capacity (CEC) of the
75 clay minerals and low sorption affinity for most cations, primarily hydrated divalent cations (Hinton et al.,
76 2006; Mitchell and Soga, 2005). Previous studies have concluded that HIV contributes most of the CEC in
77 the clay fraction at SRS (Goto et al., 2014). These mineral grains possess numerous nondiscriminatory
78 sites on planar surfaces and a limited number of highly selective sites at the interlayer wedge zones
79 (Goto et al., 2014, 2008). There are two types of sites associated with interlayer wedge zones, the first
80 holds cesium strongly during exchange with other cations, while the second site is located deep within
81 the interlayer wedge zone and does not readily exchange the cesium held at these sites, leading to
82 effectively irreversible attenuation of cesium over long time scales (Goto et al., 2014).

83 Additional sediment constituents impact cation sorption. Based on XRF data, iron is present in
84 the SRS sediment, comprising 2.64% of the sediment by weight (Table S3). It is unlikely that clay minerals
85 alone could make up this iron weight fraction. Studies have identified a mix of hematite and goethite
86 phases as well as a small fraction of phyllosilicate-bound iron, yielding conceptual models that include
87 iron present as goethite, hematite, or ferrihydrite (Kaplan, 2021; Kaplan et al., 2010; Peruski et al., 2017).
88 Additional details pertaining to measurements and properties of the sediments can be found in previous
89 works (Montgomery et al., 2017; Roberts et al., 2012). Oxides and oxyhydroxides contribute limitedly to
90 CEC since they possess sorption sites in the same range as kaolinite (Dragun, 1988). However, previous
91 works have concluded that these minerals provide substantial sorption sites for select cations (Kim et al.,
92 2006; Krupka and Serne, 2002; McLaren et al., 1986; Naveau et al., 2005). Although quartz represents a
93 substantial fraction of the SRS sediment by mass, it does not provide considerable cation sorption sites
94 (Aldahan et al., 1999; Dixon et al., 1989). Cation sorption is not only dependent on the presence of
95 materials capable of adsorption but also on the physiochemical properties of the system.

96 At the SRS and other areas where radioactive materials are stored, engineered systems are
97 added to limit the mobility of radionuclides. Cementitious materials are commonly used to encapsulate
98 low-level and intermediate-level radioactive wastes for disposal in near-surface geologic deposits (Goo et
99 al., 2021; Li and Pang, 2014; Tits et al., 2003). Formulations that include Portland cement are typically
100 used due to its availability, low cost, high strength, high durability, radiation stability, and the capability
101 to immobilize a wide range of waste species (Chen et al., 2009; Komljenović et al., 2020; Matsuzuru et
102 al., 1977). Mineral phases possess a high density of sites capable of radionuclide adsorption and
103 incorporation reactions, which can limit radionuclide migration (Ochs et al., 2016). However, Portland

104 cement has been shown to be ineffective for cesium and tritium (Goñi et al., 2006). To improve the
105 formulation, blast furnace slag (BFS), is added to reduce overall porosity, increase durability, enhance
106 retention via the formation of insoluble sulfide precipitates, and enhance the sorption and precipitation
107 of redox-sensitive contaminants which results in a more advantageous material with higher resistance to
108 chemicals and lower water permeability (Matsuzuru et al., 1977; Seaman and Chang, 2013).
109 Furthermore, the addition of BFS incorporates ferrous iron and sulfide (Arai et al., 2018, 2017a, 2017b;
110 Kaplan et al., 2008; Powell and Arai, 2015). Ferrous iron creates reducing conditions, which result in
111 redox-sensitive radionuclides in less mobile oxidation states, while sulfides also contribute to reducing
112 conditions, but also are precipitating agents that bind certain radionuclides as insoluble species,
113 ultimately limiting mobility from the wasteform (Andersson et al., 1983; Gilliam et al., 1990; Kaplan et
114 al., 2008). In general, higher salinity pore fluids can increase the leaching of radionuclides from
115 cementitious wasteforms over long-term timescales; however, this effect has been observed to be less
116 pronounced in reducing grout relative to Portland cement (Matsuzuru et al., 1977).

117 Cementitious leachate has very different chemical properties than background SRS groundwater.
118 Typical pH and ionic strength values for background SRS groundwater under natural conditions are 5.5
119 and 0.1 mM, respectively (Kaplan et al., 2017). The current conceptual model for the SRS clayey
120 sediment impacted by cementitious leachate (Portland cement and reducing grout) describes a
121 porewater environment with pH 2 times greater (2 orders of magnitude fewer protons) and ionic
122 strength 150 times greater, relative to that of background conditions (Kaplan, 2021). Cement leachate
123 has concentrations of competing cations, 1 to 3 orders of magnitude greater than the background
124 conditions (Kaplan, 2021). Previous studies have observed that relative to background conditions, the
125 conditions induced by the cementitious leachate substantially decrease the sorption of alkali metals but
126 yield the opposite effect in alkaline earth metals, cobalt, and europium (Jeong et al., 1998; Semenkova et
127 al., 2023; Woodward et al., 2018). The pH of the system has a significant impact on sorption of many
128 cations to sediments (Clark et al., 1998; King, 1988; Krupka and Serne, 2002; Landry et al., 2009;
129 Narendrula et al., 2012; Payne et al., 2009; Spark et al., 1995). The ionic strength of the aqueous phase
130 provides insight into the concentration of competing cations (Na^+ , K^+ , Mg^{2+} , Ca^{2+}) present. However, the
131 degree to which these cations can compete with radionuclides for sorption sites depends on the
132 selectivity of the sediments for cations. The ionic potential or the ratio of the charge to the ionic radius
133 (z/r) can also be used to predict the selectivity of sediments; cations with larger ionic potential are
134 preferentially electrostatically adsorbed over those with smaller ionic potentials (Langmuir, 1997;
135 Sposito, 1989). Other factors, such as sediment properties (Goto et al., 2014) and the hydrated radius of
136 the cation (Zaunbrecher et al., 2015), contribute to selectivity, but typically, the orders for monovalent
137 and divalent cations follow $\text{Cs}^+ > \text{Rb}^+ > \text{K}^+ > \text{Na}^+ > \text{Li}^+$ and $\text{Ba}^{2+} > \text{Sr}^{2+} > \text{Ca}^{2+} > \text{Mg}^{2+}$, respectively (Dragun, 1988). A
138 complete table of hydrated radii, ionic potential, and hydration energies is provided in the
139 supplementary material (Table S5).

140 The distribution coefficient (K_D) is the most common and simplest way to describe partitioning to
141 sediments (Dragun, 1988; Sposito, 1989). The K_D is an empirically derived construct defined as the ratio
142 of contaminant concentrations in the solid phase to the amount remaining in the aqueous phase at
143 equilibrium (Dragun, 1988; Sposito, 1989). A high K_D value indicates a high degree of sorption to
144 sediments. Additionally, the K_D can be used to describe the migration rate of a contaminant in relation to
145 the flux of the aqueous phase through the subsurface (Dragun, 1988; Sposito, 1989). Measured K_D values
146 for different contaminants vary greatly due to the dependence on the chemical properties of the

147 contaminant, aqueous phase, and solid phase (Dragun, 1988; Sposito, 1989). Therefore, it is necessary
148 to develop site-specific K_D values. Fortunately, a recent literature review has compiled data from sorption
149 studies, primarily laboratory batch (ad)sorption studies, specific to SRS materials and provides the best
150 estimates of K_D values (Kaplan, 2021). Based on Kaplan's K_D values, under the three systems analyzed in
151 this work, the affinity of the four radionuclides to undergo cation exchange is expected to vary. The
152 affinity of ^{152}Eu remains consistently high across all systems. However, in cementitious wasteforms, the
153 affinity of ^{60}Co and ^{133}Ba is expected to increase by one to two orders of magnitude compared to the
154 sediment control, while the affinity of ^{137}Cs is anticipated to decrease an order of magnitude (Table S1).

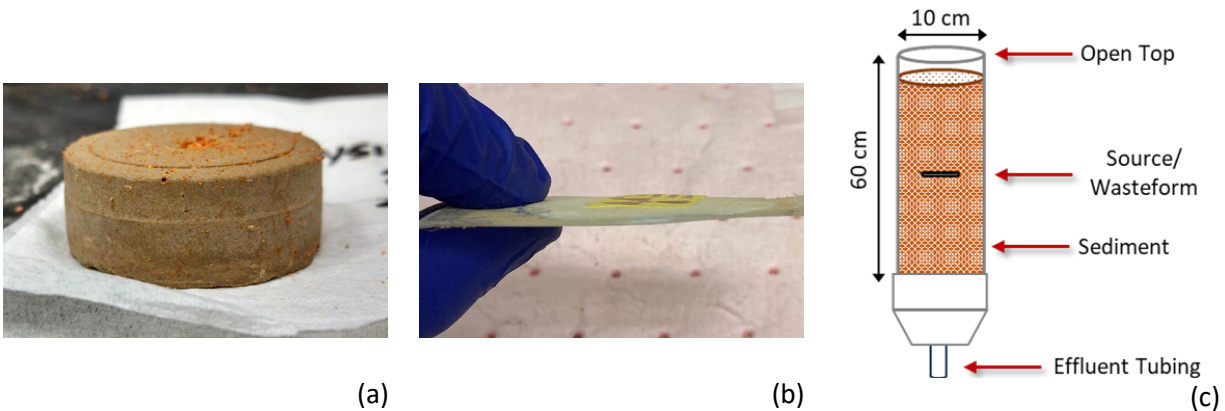
155 The composition of the sediment and the wasteform used for radionuclide disposal can both
156 impact radionuclide mobility and, ultimately, migration through the subsurface. This work seeks to
157 improve upon an existing non-destructive gamma-ray spectrographic technique and demonstrate the
158 ability of this technique to reliably monitor the migration of radionuclides through lysimeter columns
159 over several years. Select radionuclides were incorporated into cementitious grouts, placed within field
160 lysimeters, and left for exposure to natural rainfall and temperature fluctuations for 10 years. The non-
161 destructive approach allowed the radionuclide distribution to be determined after 4 years of deployment
162 in a previous study (Erdmann et al., 2018) and again after 10 years in the current work. This study will
163 provide insight into the impact of different cementitious wasteform formulations on the distribution of
164 radionuclides after a decade of field deployment and present a novel detection approach for non-
165 destructive analysis of gamma-emitting isotopes. This non-destructive approach allows for multiple
166 measurements of radionuclide distributions over time in mesoscale field studies, which can be used to
167 monitor leaching from wasteforms and transport through sediments.

168 2. Methods and Materials

169 Lysimeters containing sources amended with a suite of gamma-emitting radionuclides (^{137}Cs ,
170 ^{60}Co , ^{133}Ba , and ^{152}Eu) were deployed for approximately 10 years in the field at the RadFLEX facility at the
171 United States Department of Energy SRS. This work serves as a follow-up to a study conducted in 2016,
172 which non-destructively measured the concentration of each radionuclide in the sediment column as a
173 function of depth after 4 years of deployment in the field (Erdmann et al., 2018). Following the
174 measurement, one lysimeter was destructively analyzed to confirm the results, and the remaining
175 lysimeters were redeployed in April 2017, recovered in December 2021, and similarly analyzed in 2022 to
176 determine the extent of transport after another 4 years of deployment. A duplicate lysimeter to the one
177 destructively analyzed in 2017 was measured in the present study. A concise outline of the deployment
178 periods for each lysimeter is provided in Table S6.

179 The analyzed lysimeters contain the gamma suite incorporated into cementitious pucks (Portland
180 cement or reducing grout) or introduced into the sediment via a filter paper "pita pocket" as a sediment
181 control (*i.e.*, exposed to natural site conditions). The sediment control was used to monitor radionuclide
182 transport through the sediment without any influence of a wasteform or ions leaching from the
183 wasteforms. The source material type is included in the lysimeter naming scheme, except for the
184 sediment control, and the subsequent number refers to the replicate number (Table 2). Sediment
185 Control-1 refers to the lysimeter that was destructively analyzed in 2017, and Sediment Control-2 is the
186 identical duplicate measured in the current study. The pita pockets are approximately 4.7 cm in diameter,
187 0.1 cm thick, and were constructed by stitching together two Whatman glass fiber filters with Teflon
188 thread (Roberts et al., 2012). Each of the cementitious wasteform pucks was created by mixing a salt

189 solution containing the radionuclides with dry Portland cement, blast furnace slag, and fly ash using a 0.6
190 g salt solution to 1 g dry mix ratio as described by Roberts *et al.*, (2012). The Portland cement source was
191 55% Portland cement and 45% fly ash, and the reducing grout was 45% fly ash, 45% blast furnace slag,
192 and 10% Portland cement. The cementitious pucks have a diameter of 3.18 cm and a thickness of 1.27
193 cm (Roberts *et al.*, 2012). The differences in the thickness of the sources are displayed in Fig. 1. Each
194 lysimeter is composed of an open-top 60-cm by 10-cm (ID) PVC pipe to allow for precipitation to impact
195 the sediments via infiltration and evaporation (Fig. 1). The bottoms of the lysimeters were fitted with a
196 mesh screen, reducer, and tubing to allow effluent collection and analysis (Erdmann *et al.*, 2018; Roberts
197 *et al.*, 2012). The sediments used in these experiments are representative of the SRS vadose zone
198 (characteristics provided in Table S2). Prior to field implementation, the lysimeters were filled with
199 approximately 50 cm of the SRS vadose zone sediment, and one of the sources was situated at a height
200 of approximately 25 cm. The constituents were added to the lysimeters as follows: sediment to a height
201 of 25 cm, tamped to induce settling, wasteform, an additional 25 cm of the same sediment, and tamped.
202 For each lysimeter, the source material type and the initial activity present are listed in Table 1. Previous
203 works have provided additional details pertaining to the lysimeter design and configuration (Kaplan *et al.*,
204 *et al.*, 2017; Roberts *et al.*, 2012; Santikari *et al.*, 2022).



205 Fig. 1. Images of a cementitious wasteform (a) and a side-view of the filter paper source (b) and a
206 schematic drawing of a lysimeter column (c).

Table 1. Lysimeter, the source material, initial activity added, and the activity added decay corrected to the time the scans were conducted for the current study.

Lysimeter	Source Material	Initial Activity (MBq)				Decay Corrected Activity (MBq)			
		¹³⁷ Cs	⁶⁰ Co	¹³³ Ba	¹⁵² Eu	¹³⁷ Cs	⁶⁰ Co	¹³³ Ba	¹⁵² Eu
Portland Cement-1	Portland Cement	4.68	5.09	3.97	9.40	3.70	1.33	2.03	5.57
Reducing Grout-1	Reducing Grout	4.68	5.09	3.97	9.40	3.70	1.33	2.03	5.57
Sediment Control-1	Filter Paper	0.29	0.32	0.25	0.47	<i>Destructively analyzed in 2017</i>			
Sediment Control-2	Filter Paper	0.29	0.32	0.25	0.47	0.23	0.08	0.13	0.28

207

208 2.1. Detection System

209 A custom-built system capable of using a high-purity germanium detector to conduct automated
 210 scans of lysimeter columns with a spatial resolution of 0.2 cm was designed for these tests (Erdmann et
 211 al., 2018). The detection system was calibrated using Spectrum Technologies beta/gamma disk sources
 212 and a standard created using a NIST traceable ¹⁵²Eu solution. Additionally, the detection efficiency of the
 213 system was determined using the same ¹⁵²Eu solution incorporated into a cementitious wasteform and
 214 background was determined by analyzing a blank lysimeter filled with only clean SRS Sediment. Erdmann
 215 *et al.*, (2018) provides a detailed description of the detection system and associated calibration.

216 In the current study, duplicate scans of Reducing Grout-1 and Sediment Control-2 and triplicate
 217 scans of Portland Cement-1 were conducted to reduce the impact of heterogeneities and source
 218 placement on the detected radionuclide spatial distribution. Lysimeters were initially scanned on a
 219 shorter time interval with coarse spacing between measurement areas to estimate the height, or
 220 location, of the source and the extent of the region containing activity above the background. After
 221 determining the general location of the source, the automated detection system was programmed to
 222 measure the lysimeter at 0.2 cm intervals over a range approximately 7 cm above and below the source.
 223 Each interval was counted for 1800 seconds, except when measuring Sediment Control-2, the count time
 224 was extended to 7200 seconds due to the lower activity present in the source. For example, if a
 225 cementitious wasteform was determined to be present at a height of 27 cm, the system was
 226 programmed to count every 0.2 cm from 20 cm to 34 cm, resulting in 101 individual measurements over
 227 roughly 2 days. After completing the first scan of the lysimeter, the lysimeter was rotated 180 degrees,
 228 and the system was restarted with no adjustments to the counting parameters. After the second scan of
 229 Portland Cement-1, the lysimeter was rotated 90 degrees, and the measurement was conducted again.

230 2.2. Data Analysis

231 After the scans were completed, Microsoft Excel was used to determine the net peak areas from
 232 the detection system output files. The gross counts were plotted as a function of the channel to view the
 233 photopeaks. To account for the increased baseline due to Compton scattering, the counts of roughly the
 234 10 channels to the left and right of the photopeak of interest were averaged, and then this area was
 235 subtracted from the total area under the photopeak curve. The number of neighboring channels varied
 236 slightly between the photopeaks of interest due to the proximity of other spectrum features. The
 237 counting interval with the highest activity was assumed to be the source location and assigned a height
 238 of 0 cm. The intervals above and below this point were incrementally assigned values starting at 0.2 cm
 239 and -0.2 cm, respectively. The duplicate datasets were then averaged to create one dataset for each of
 240 the lysimeters. The average activity distribution profiles were analyzed to quantify the migration of the
 241 radionuclides through the sediments. Since the initial activity incorporated into the cementitious
 242 wastefoms and the filter paper sources differed by an order of magnitude, the activity present at each
 243 scanning interval was normalized using the total activity added to the source decay corrected for the
 244 time of the measurement. It is important to note that the cementitious wastefoms are 1.27 cm tall,
 245 while the height of the filter paper source is roughly 0.1 cm.

246 3. Results and Discussion

247 Overall, the redeployment period (2017-2022) resulted in increased migration of the four
 248 radionuclides regardless of the source type. Generally, effluent volume over time was consistent with
 249 expected rainfall variability over the length of the experiment. The normalized activity distributions
 250 developed from the lysimeter scans are displayed in Figs. 2, 3, 4, and 5, and Table 2 contains the
 251 percentage of the normalized activity remaining in the approximate source region at the time of the
 252 2016 and 2022 measurements. All of the values are averages of the duplicate or triplicate scans
 253 performed on each lysimeter; within the approximate source regions, the standard deviations were no
 254 greater than 25% of the average value. When comparing the percentages between the different
 255 measurement years, it is noteworthy that the spatial resolution of the scans differed between the years.
 256 The spatial resolutions were 0.254 cm and 0.2 cm for 2016 and 2022, respectively. The 2016 resolution
 257 yielded approximate source regions covering a vertical distance of 1.27 cm for the cementitious
 258 wastefoms and 0.254 for filter paper sources, respectively. With the 0.2 cm step size used in the current
 259 work, the region of the 1.27 cm tall wastefom had to be approximated in 0.2 cm steps, resulting in a
 260 total wastefom region height in the data of 1.4 cm compared with the exact value of 1.27 cm using the
 261 0.254 cm step length by Erdman *et al.*, (2018).

262 Table 2. Percentage of radionuclide present in the approximate source region (decay corrected).

Radionuclide	Portland Cement-1		Reducing Grout-1		Sediment Control-1	Sediment Control-2
	2016	2022	2016	2022	2016	2022
⁶⁰ Co	94	63	96	63	14	8
¹³³ Ba	88	65	96	80	12	5
¹³⁷ Cs	41	37	64	53	26	11
¹⁵² Eu	96	78	97	85	35	16

263 3.1. Cobalt

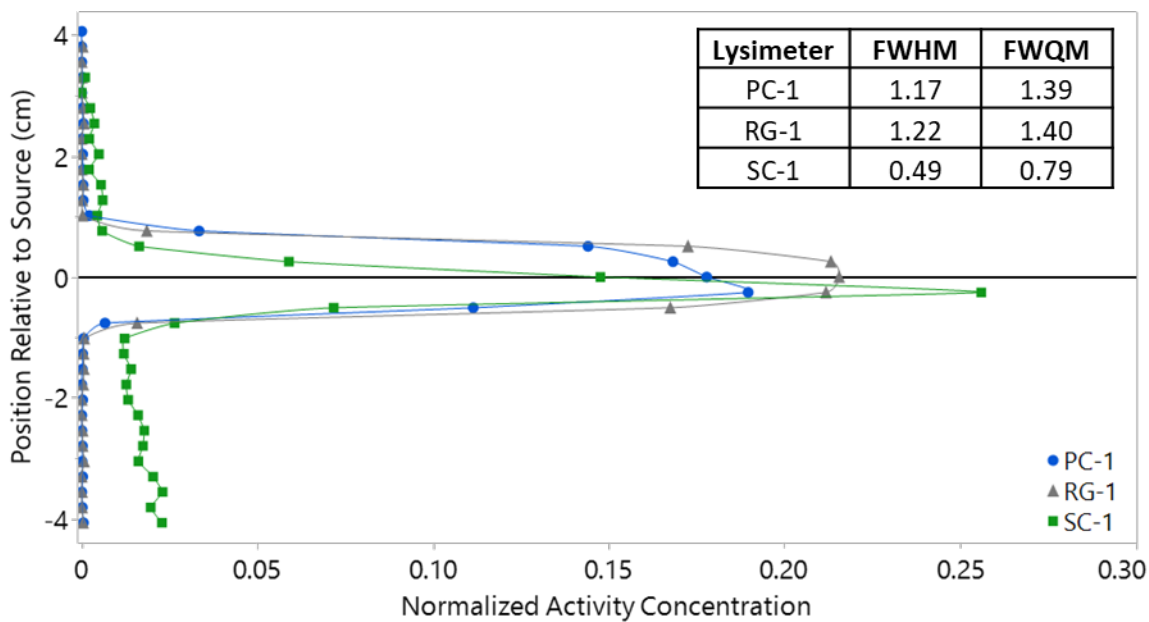
264 The ^{60}Co normalized activity distributions detected during the 2022 measurements for Portland
265 Cement-1, Reducing Grout-1, and Sediment Control-2 were nearly identical from the top of the counting
266 area (4 cm above the source center) to 1 cm below the source center (Fig. 2 (b)). However, beyond 1 cm
267 below the source center, and continuing through to the lowest measurement of the lysimeters (6.6 cm
268 below the source center), the normalized activity in Sediment Control-2 was elevated relative to the
269 cementitious sources. At 1 cm below the source centers, normalized activities of 0.019, 0.026, and 0.034
270 were measured for Portland Cement-1, Reducing Grout-1, and Sediment Control-2, respectively. From 1
271 to 2 cm below the approximate source center, the normalized activities in all three lysimeters declined
272 approximately exponentially until reaching a constant value of 0.002 for both cementitious lysimeters
273 and 0.015 for Sediment Control-2. The ratios of FWHM/FWQM (FWHM = full width at half maximum of
274 the activity distribution in the lysimeter, FWQM = full width at quarter maximum of the activity
275 distribution in the lysimeter) were identical in Portland Cement-1 and Reducing Grout-1 (0.69). However,
276 a lower ratio (0.59), indicating increased spreading, was observed in Sediment Control-2 (Fig. 2).
277 Furthermore, the same trend was observed for the 2016 measurements. Overall, the ratios decreased
278 between the 2016 and 2022 measurements. Therefore, the peaks became shorter and wider during the
279 redeployment, indicating that a smaller fraction of the radionuclides remained in the approximate
280 source area and that the extent of migration increased.

281 Recall that the height of the source materials (cementitious puck vs filter paper) varied by more
282 than an order of magnitude. Thus, if the migration of ^{60}Co at the time of the 2022 measurements is
283 considered from the edge of the approximate source region, the distributions for the cementitious
284 wastefoms are nearly identical, while in Sediment Control-2, the distribution of normalized activity is
285 roughly two-fold greater above -1 cm and an order of magnitude greater below -1 cm. At the time of the
286 2022 measurements, Reducing Grout-1, Portland Cement-1, and Sediment Control-2 the approximate
287 wasteform regions contained 63.4, 63.0, and 8.3% of the initial ^{60}Co activity, respectively. Measurements
288 of ^{60}Co in the Portland Cement-1 effluent have been observed to be the highest cumulative activity of
289 the radionuclides analyzed in the study (Fig. S4). To account for the difference in the initial activity added
290 to the cementitious and filter paper sources, the cumulative ^{60}Co activity in the effluent has been
291 normalized by the initial activity, yielding values for Portland Cement-1 and Reducing Grout-1 two and
292 three orders of magnitude greater than that for Sediment Control-2, respectively. Considering the
293 different analyses, little difference between the cementitious wastefoms was observed for retention in
294 the wasteform and distribution in the lysimeter. However, the activity measured in the effluent for
295 Portland Cement-1 was an order of magnitude greater than Reducing Grout-1. Although less ^{60}Co was
296 maintained in the filter paper source, and ^{60}Co was observed to migrate further in Sediment Control-2,
297 lower cumulative activity was measured in the effluent. Many of the measurements of other
298 radionuclides in the effluent over the 10-year monitoring period were at or below detection limits. It is
299 noteworthy that a factor of ~ 16 less activity was added to the sediment control lysimeters relative to
300 cementitious lysimeters. Of all the radionuclides, the highest activities in the effluent were measured for
301 ^{60}Co during the first two years of deployment, particularly in Portland Cement-1 (Fig. S4). The initial ^{60}Co
302 pulse observed primarily in Portland Cement-1, but also to a lesser extent in Reducing Grout-1, coincides
303 with pulses of sodium (Fig. S3). However, it is not fully understood what caused the initial ^{60}Co pulse.

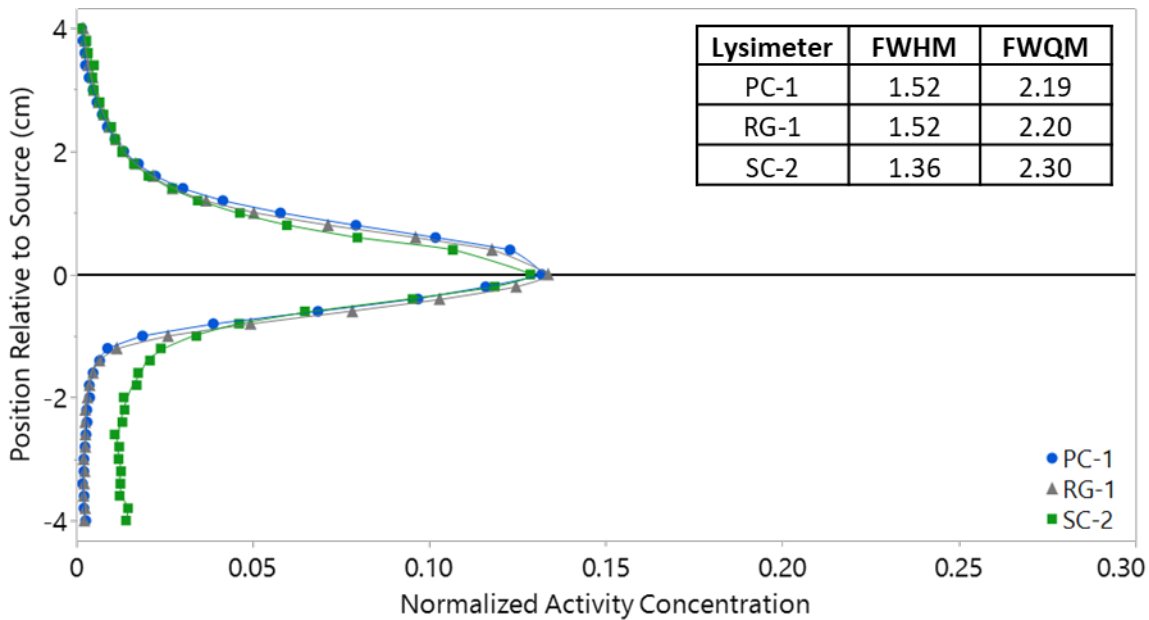
304 Cobalt (II) has a high potential for mobility due to its high solubility in water (Woodward et al.,
305 2018). Properties observed to have the greatest impact on cobalt sorption, in no order, are exchangeable
306 calcium, pH, and CEC of the sediment (Kim et al., 2006). Soil oxides (ferrihydrite) provide the most

307 significant sorption sites for cobalt, followed by mineral oxides, while clay minerals have limited impact
308 (Kim et al., 2006; Krupka and Serne, 2002; McLaren et al., 1986). Albeit, SRS sediments contain cation
309 exchange sites, sorption at these sites is competitive and pH-dependent (Payne et al., 2009). The pH_{PZC}
310 for ferrihydrite, goethite, hematite, and kaolinite are 8.1 (Mendez and Hiemstra, 2020), 7.8 (Benjamin,
311 2015), 8.5 (Benjamin, 2015), and 4.6 (Benjamin, 2015). Thus, under background conditions at SRS
312 (Sediment Control-1 and Sediment Control-2), the most significant sorption surfaces are largely
313 positively charged and thus weakly attract cobalt. These factors are thought to result in the observed
314 enhanced mobility of ^{60}Co relative to the others.

315 The incorporation of the radionuclide suite in a cementitious wasteform, as compared to the
316 sediment control, altered the migration of ^{60}Co through the lysimeters. It is hypothesized that low
317 solubility solids can precipitate in the cementitious pucks. These may be hydroxides and carbonate,
318 capable of cobalt co-precipitation (Brooks et al., 1998; Kim et al., 2006). Alternatively, Yoon *et al.*, (2020)
319 identified cobalt precipitated as a cobalt-sulfide in the presence of a grout containing blast furnace slag,
320 an ingredient in the Reducing Grout-1 wasteform. In this study, little difference was observed in the
321 cobalt distributions of Portland Cement-1 and Reducing Grout-1 despite the addition of blast furnace
322 slag to Reducing Grout-1. However, fly ash, which potentially contains sulfides, was added to both
323 cementitious wasteforms. Once leached from the wasteform migration of cobalt will be dominated by
324 ion exchange processes. The total activity measured in the effluent was an order of magnitude lower for
325 Reducing Grout-1 relative to Portland Cement-1 (Fig. S4 (d)). The contributions to the total activity in the
326 effluent primarily occurred during the first two years of the experiment, and during this time period, the
327 sodium concentrations were an order of magnitude higher in the effluent for Reducing Grout-1 and
328 Portland Cement-1 relative to Sediment Control-2. The higher effluent concentrations were likely due to
329 the higher dissolved ion concentrations, because in the 4-6.5 pH range, ion exchange dominates cobalt
330 sorption, and thus the fraction adsorbed depends on the ionic strength of the solution (Landry et al.,
331 2009). The decreased spreading observed in Portland Cement-1 and Reducing Grout-1 relative to
332 Sediment Control-1 and Sediment Control-2, is consistent with the current best estimates for the K_D
333 values (Table S1).



334



335

336 Fig. 2. The distributions of ^{60}Co activity as a function of distance from the approximate center of the
 337 source in (a) 2016 and (b) 2022. (PC-1 = Portland Cement-1, RG-1 = Reducing Grout-1, SC-1 = Sediment
 338 Control-1, SC-2 = Sediment Control-2, FWHM = full width at half maximum of the activity distribution in
 339 the lysimeter, FWQM = full width at quarter maximum of the activity distribution in the lysimeter). The
 340 plots illustrate the ^{60}Co activity normalized by the decay-corrected initial activity added to the lysimeters
 341 as a function of depth in the lysimeters. A depth of zero was assigned to the approximate center of the
 342 source. Note that only an 8 cm section is being shown of the 56 cm sediment column to demonstrate the
 343 differences between the systems surrounding the source region. Note that the lines connecting the data
 344 points are simply for guidance.

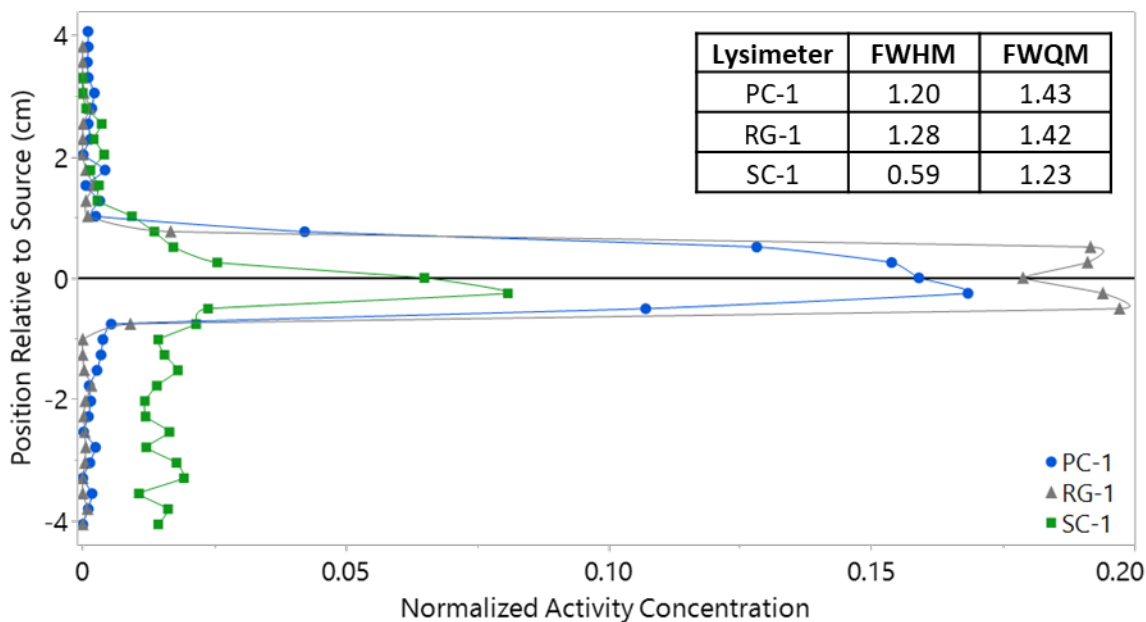
345 3.2. Barium

346 Barium-133 distributions in Portland Cement-1 and Reducing Grout-1 were similar and nearly
347 symmetrical above and below the wasteform in 2016 and 2022 (Fig. 3). However, in both datasets, the
348 normalized activity peak for Portland Cement-1 was shorter than that of Reducing Grout-1, indicating a
349 higher degree of migration in Portland Cement-1 than in Reducing Grout-1. Furthermore, the
350 FWHM/FWQM ratio of the activity distribution in the lysimeter for Reducing Grout-1 was 0.90 and 0.81
351 for 2016 and 2022, respectively (Fig. 3). Whereas the ratio for Portland Cement-1 was 0.84 in 2016 and
352 0.74 in 2022. The peaks of the normalized activity distributions for the cementitious wasteforms were
353 twice the height of the peaks measured for Sediment Control-1 in 2016 and Sediment Control-2 in 2022.
354 Additionally, the FWHM/FWQM ratio for Sediment Control-1 was 0.48 in 2016 and the ratio for Sediment
355 Control-2 in 2022 was 0.14. These results suggested that some factors of the cementitious wasteforms
356 decreased radionuclide transport between sampling periods. Unlike the cementitious wasteforms, the
357 1D scans revealed asymmetric activity distributions for Sediment Control-1 and Sediment Control-2,
358 indicating more downward than upward movement of ^{133}Ba . Overall, the scans of Sediment Control-1
359 and Sediment Control-2 revealed similarly shaped activity distributions, although four additional years of
360 deployment resulted in a peak roughly half as tall and a 66% increase in the normalized activity
361 concentration below the source in Sediment Control-2. The percent decrease of the normalized activity
362 present in the Sediment Control-2 approximate source region was roughly twice that observed in the
363 cementitious wasteforms.

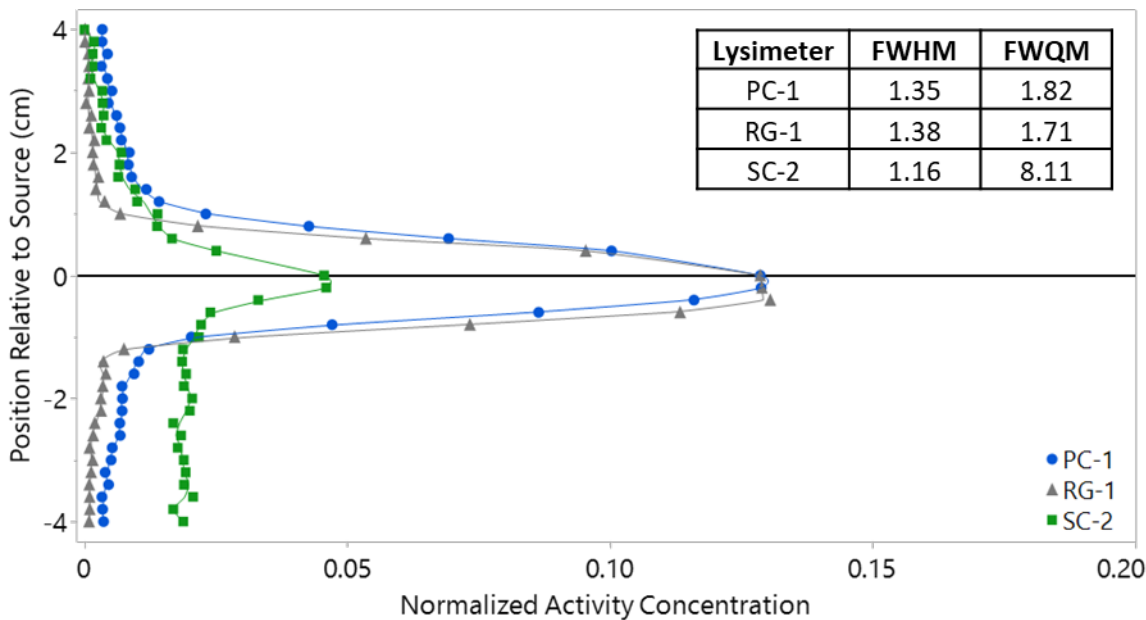
364 Based on the information provided by the 1D scans in 2016 and 2022, the greatest migration of
365 ^{133}Ba occurred in Sediment Control-1, followed by Portland Cement-1, and then Reducing Grout-1. When
366 considering the extent of migration from the edge of the source rather than the center, the same order is
367 observed, but the variance between the materials is more substantial. Although the distributions for
368 Portland Cement-1 and Reducing Grout-1 appear similar, in the region outside the wasteform, the
369 normalized activity as a function of depth is 2 to 5-fold greater in Portland Cement-1. Furthermore, the
370 cumulative activity in the effluent normalized to the initial activity added to the source increased in the
371 order Reducing Grout-1<Portland Cement-1<Sediment Control-2, with an order of magnitude separating
372 each rank (Fig. S4 (c)). Additionally, the calculation of ^{133}Ba activity remaining in the approximate source
373 region revealed a higher percentage remaining in Reducing Grout-1 than Portland Cement-1, while the
374 percentage for Sediment Control-2 was more than an order of magnitude lower than the cementitious
375 wasteforms.

376 The primary factors impacting the migration of barium are the pH (Eylem et al., 1990), the
377 solubility of barium (Almond and Kaplan, 2011), and precipitation reactions (Almond and Kaplan, 2011;
378 Kaplan, 2021; Seaman and Chang, 2013). Kaolinite and HIV compose most of the cation exchange
379 capacity of the SRS sediments. However, barium is strongly hydrated, which limits close interaction with
380 kaolinite surfaces resulting in weak binding (Jeong et al., 1998), and hinders the ability of FES to function
381 as sorption sites for this cation (Zaunbrecher et al., 2015). Furthermore, the sorption of barium increases
382 with increasing pH, indicating that surface complexation is a contributing factor. Thus, under background
383 conditions present in Sediment Control-1 and Sediment Control-2, the SRS sediments offer limited
384 sorption capacity for ^{133}Ba . The cementitious wasteforms imposed physical and chemical conditions that
385 altered the migration ^{133}Ba in the lysimeters. These wasteforms induce alkaline conditions, which
386 previous studies have observed to slightly increase barium sorption to kaolinite (Eylem et al., 1990). The

387 elevated pH of the cementitious leachate is hypothesized to have decreased the mineral surface charge
388 of the SRS sediments relative to the background conditions in the vicinity of the cementitious
389 wasteforms, facilitating greater ^{133}Ba adsorption. However, more impactful to barium mobility is the
390 presence of carbonates and sulfates or sulfides in the cementitious leachate. These constituents can
391 trigger the formation and precipitation of barium sulfate (BaSO_4), barium sulfide (BaS), and witherite
392 (BaCO_3), all of which are largely insoluble (Kaplan, 2021; Peruski et al., 2017; Seaman and Chang, 2013).
393 Furthermore, the addition of BFS physically changes wasteforms, reducing the size of the capillary pores
394 limiting water passing through (Seaman and Chang, 2013). Previous works have observed the K_D value
395 for barium to increase in cementitious leachate, particularly reducing grout, suggesting that the higher
396 sulfide content of the cementitious wasteforms is an important parameter limiting migration (Almond
397 and Kaplan, 2011; Seaman and Chang, 2013). Thus, it is hypothesized that the addition of BFS minimized
398 ^{133}Ba leaching from the Reducing Grout-1 wasteform at the time of the 2022 scans. The overall extent of
399 ^{133}Ba migration in the lysimeters is consistent with the current best estimates of the K_D values (Table S1).



400 (a)



401 (b)

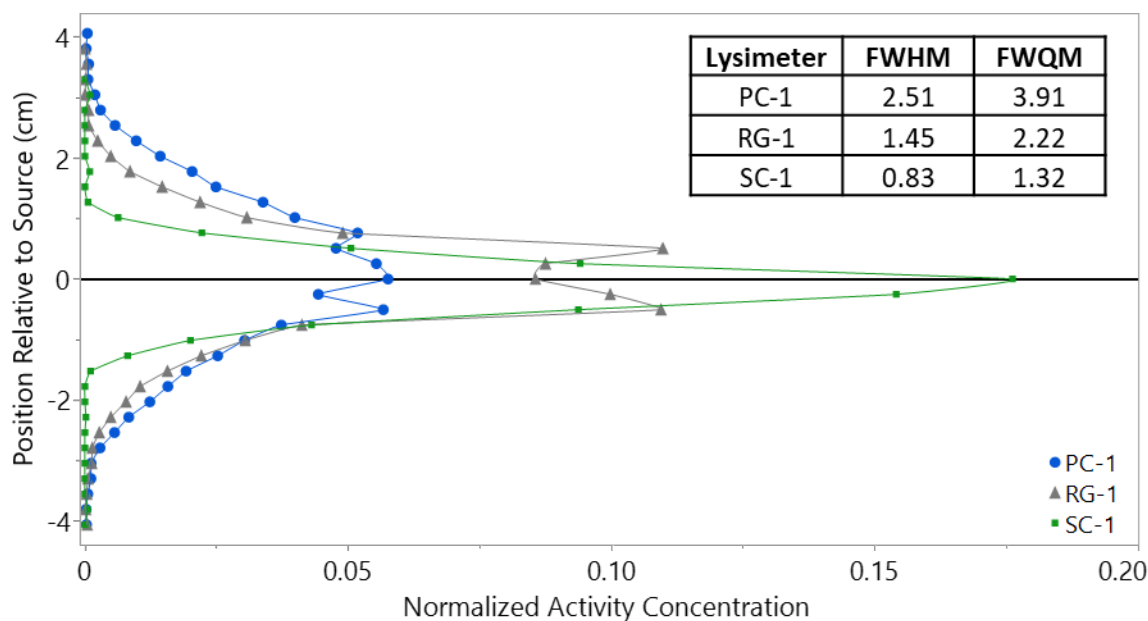
402 Fig. 3. The distributions of ^{133}Ba activity as a function of distance from the approximate center of the
 403 source in (a) 2016 and (b) 2022. (PC-1 = Portland Cement-1, RG-1 = Reducing Grout-1, SC-1 = Sediment
 404 Control-1, SC-2 = Sediment Control-2, FWHM = full width at half maximum of the activity distribution in
 405 the lysimeter, FWQM = full width at quarter maximum of the activity distribution in the lysimeter). The
 406 plots illustrate the ^{133}Ba activity normalized by the decay-corrected initial activity added to the system as
 407 a function of depth in the lysimeters. A depth of zero was assigned to the approximate center of the
 408 source. Note that only an 8 cm section is being shown of the 56 cm sediment column to demonstrate the
 409 differences between the lysimeters surrounding the source region. Note that the lines connecting the
 410 data points are simply for guidance.

411 3.3. Cesium

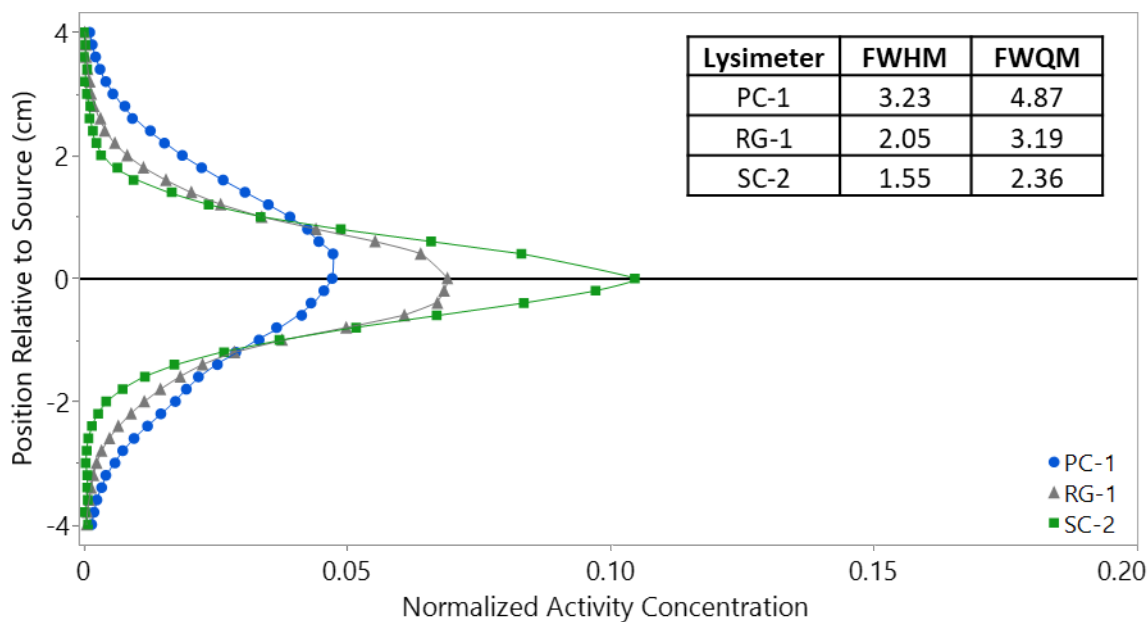
412 The scan data indicated that all measurements of the three lysimeters produced symmetric ^{137}Cs
413 normalized activity distributions that became shorter and wider compared to prior measurements. For
414 2016 and 2022 measurements, the narrowest peaks were Sediment Control-1 and Sediment Control-2,
415 followed by Reducing Grout-1 and Portland Cement-1 (Fig. 4). The FWHM/FWQM ratios of the activity
416 distribution in the lysimeter were within 0.64 ± 0.02 for the three lysimeters in 2016 and 2022, indicating
417 that the ^{137}Cs is migrating at a constant rate (Fig. 4). The 2022 1D scans demonstrated that the extent of
418 ^{137}Cs migration as a function of vertical distance from the center of the approximate source region center
419 increased in the order Sediment Control-2, Portland Cement-1, and Reducing Grout-1. The source region
420 in Sediment Control-2 contained the smallest percentage of the initial activity, roughly 11%. While the
421 Portland Cement-1 and Reducing Grout-1 wastefrom regions contained approximately 37% and 53% of
422 the initial activity, respectively. Furthermore, the normalized cumulative activity in the lysimeter
423 effluents increased in the order Reducing Grout-1<Sediment Control-2<Portland Cement-1 (Fig. S4 (b)).
424 These findings indicate that although more ^{137}Cs exited Sediment Control-2, the ^{137}Cs leaching from the
425 Portland Cement-1 wastefrom migrated further in the sediment column. This is further supported when
426 considering spreading from the source edge. Elevated activity was present in the vicinity of the sources
427 (± 0.5 cm) in Sediment Control-1 and Sediment Control-2 relative to the cementitious wastefroms, but
428 the width of the peaks at 1% of the normalized activity increased in the order of Reducing Grout-1,
429 Sediment Control-2, and Portland Cement-1. Measurements of the lysimeter effluents demonstrated
430 higher sodium concentrations when cementitious wastefroms were present (Fig. S3 (a)). It is speculated
431 that the increased ionic strength enhanced the migration of ^{137}Cs that exited the wastefrom. While the
432 2022 results suggeste that the presence of cementitious materials increased the retention of ^{137}Cs in the
433 Portland cement wastefrom, stable counter ions such as sodium and calcium lead to enhanced transport
434 of ^{137}Cs , which leaches from the wastefrom.

435 Cesium does not form an important aqueous complex with ligands or organic matter and exists
436 predominately as the Cs^+ ion in natural systems (Cantrell et al., 2007). The precipitation and
437 coprecipitation of cesium-containing solids are not important for limiting the migration of cesium due to
438 the high solubility of cesium-containing solids, and cesium does strongly sorb to many minerals (Cantrell
439 et al., 2007). Under the conditions induced by the cementitious materials, the elevated pH is expected to
440 have a negligible impact on cesium sediment sorption (Giannakopoulou et al., 2007). Thus, the most
441 important factor in the presence of cementitious materials impacting the sorption of cesium to
442 sediments is the concentration of competing cations (Jeong et al., 1998; Seaman and Chang, 2013).
443 Jeong *et al.*, (1998) demonstrated that cesium sorption to kaolinite remains relatively constant with
444 changing pH, but increasing the ionic strength decreases the fraction of cesium sorbed; indicating that
445 cesium sorption is more heavily dependent on ion exchange than surface complexation. Competing
446 cations only compete for non-discriminatory ion exchange sites on mineral surfaces (Goto et al., 2014).
447 Cesium-specific sorption sites reside in the inter-layer wedge zones of HIV; these areas are inaccessible
448 for cations with other charges or large hydrated radii, and therefore can limit the mobility of cesium even
449 in the presence of competing cations (Goto et al., 2008; Kaplan et al., 2017). Cementitious materials
450 have been observed to enhance cesium retention due to mineral phases containing a high density of
451 cation exchange sites (Ochs et al., 2016). Reducing grout can further enhance cesium retention because
452 it contains BFS, which has been observed to decrease the capillary pore size limiting the leachability of
453 cesium from cementitious wastefroms (Bar-Nes et al., 2017; Kumar et al., 1987; Matsuzuru et al., 1977).

454 Therefore, it is suspected that both cementitious materials enhanced ^{137}Cs retention within the
455 wasteforms, but the incorporation of BFS enabled the Reducing Grout-1 wasteform to retain a greater
456 fraction of ^{137}Cs than Portland Cement-1. Furthermore, the increased ionic strength in Portland Cement-
457 1 and Reducing Grout-1 reduced the number of ion exchange sites available, enhancing the migration
458 extent of ^{137}Cs that exited the wasteform. Although the ionic strength was similar for Portland Cement-1
459 and Reducing Grout-1, the ability of Reducing Grout-1 to retain a higher percentage of ^{137}Cs in the
460 wasteform mitigated the impacts of the elevated ionic strength. In the present study, migration was
461 observed to increase in the order of Reducing Grout-1<Sediment Control-2<Portland Cement-1.
462 However, based on the order of magnitude higher K_D value for the conditions in the SRS sediments
463 relative to those induced by cementitious wasteforms, it was anticipated that the ^{137}Cs migration would
464 be reduced in Sediment Control-1 and Sediment Control-2 relative to the cementitious wasteforms
465 (Table S1). Although, the results of this study are unable to conclusively determine the factors that
466 contributed to the migration extent in each lysimeter, it is speculated that the concentration of highly
467 selective sites for ^{137}Cs , the ability of the wasteform to retain ^{137}Cs , and the ionic strength of the pore
468 waters contributed.



469



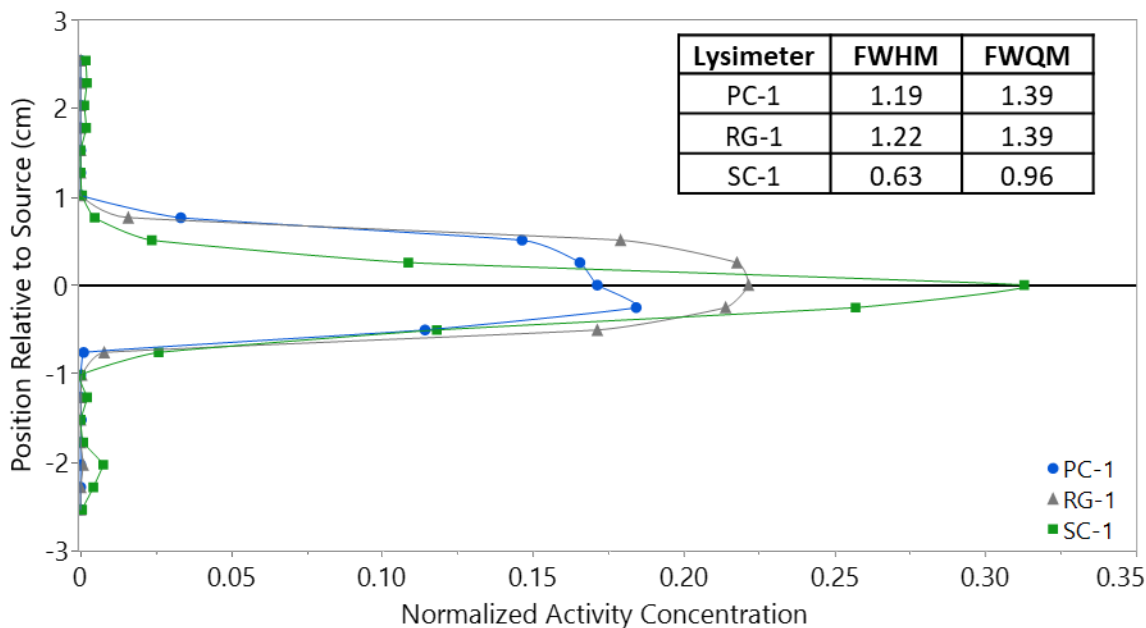
470

471 Fig. 4. The distributions of ^{137}Cs activity as a function of distance from the approximate center of the
 472 source in (a) 2016 and (b) 2022. (PC-1 = Portland Cement-1, RG-1 = Reducing Grout-1, SC-1 = Sediment
 473 Control-1, SC-2 = Sediment Control-2, FWHM = full width at half maximum of the activity distribution in
 474 the lysimeter, FWQM = full width at quarter maximum of the activity distribution in the lysimeter). The
 475 plots illustrate the ^{137}Cs activity normalized by the decay-corrected initial activity added to the system as
 476 a function of depth in the lysimeters. A depth of zero was assigned to the approximate center of the
 477 source. Note that only an 8 cm section is being shown of the 56 cm sediment column to demonstrate the
 478 differences between the lysimeters surrounding the source region. Note that the lines connecting the
 479 data points are simply for guidance

480 3.4. Europium

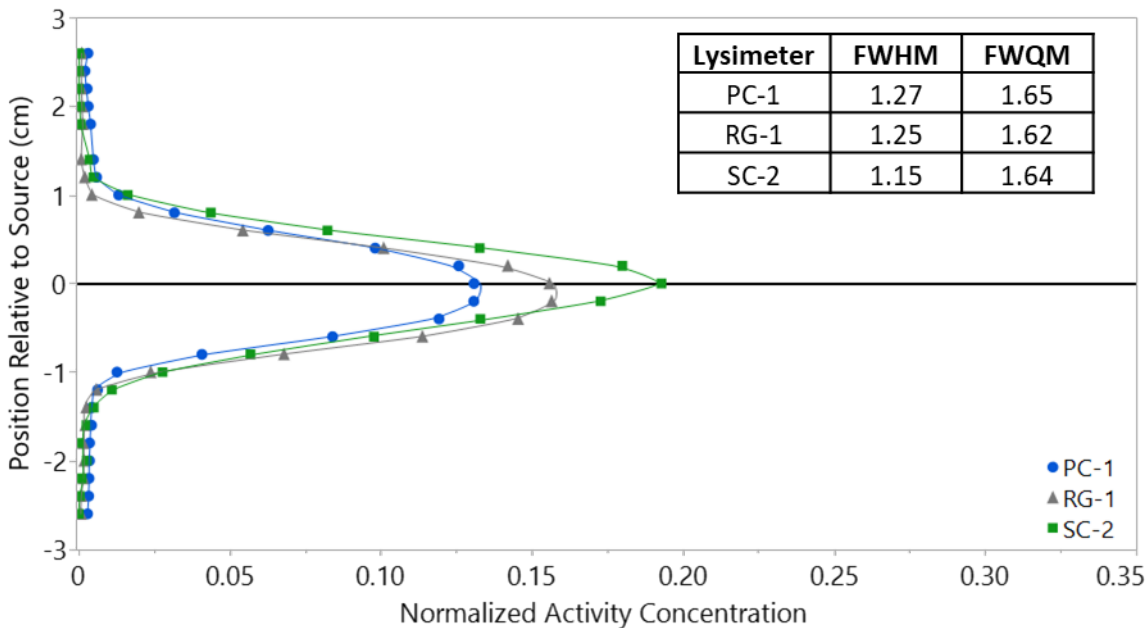
481 The most recent lysimeter measurements identified nearly symmetric ^{152}Eu normalized activity
482 distributions (Fig. 5 (b)). Similar peaks were observed in the scans from the 2016 study; however,
483 following the redeployment period, the peaks became shorter and wider (Fig. 5 (a)). The FWHM/FWQM
484 ratios of the activity distribution in the lysimeter in 2016 for Portland Cement-1, Reducing Grout-1, and
485 Sediment Control-1 were 0.85, 0.88, and 0.66, respectively (Fig. 5). For the 2022 measurements, the
486 ratio for Portland Cement-1 was 0.77, Reducing Grout-1 was 0.77, and Sediment Control-2 was 0.70. This
487 trend indicates that the activity present at the center of the source is decreasing while the activity
488 present in areas outside the source is increasing. In both studies, the peaks increased in height and
489 decreased in width in the order of Portland Cement-1, Reducing Grout-1, and Sediment Control-1/2. This
490 suggests that there is less spreading in the sediment control lysimeter, but at the time of the 2022 scans,
491 the percentage of the initial activity remaining in the approximate source region was roughly five times
492 lower for Sediment Control-2 relative to the two cementitious wastefoms (Table 2). Thus, it is
493 imperative to consider the spreading of the peaks from the edge of the approximate source region
494 rather than the center. The normalized activity in the 0.5 cm region below the Reducing Grout-1
495 wastefom was twice that of Portland Cement-1. When considering the entire approximate source
496 region, the highest percentage of the initial activity remained in Reducing Grout-1 during both the 2016
497 and 2022 studies. Consistent with the 1D distributions and the activity remaining in the approximate
498 source regions, the normalized activities in the effluents were nearly identical for Portland Cement-1 and
499 Reducing Grout-1, while an order of magnitude higher for the Sediment Control-2 (Fig. S4 (a)). These
500 findings indicate that the cementitious materials decreased the migration of ^{152}Eu in the lysimeter
501 columns.

502 Generally, under the conditions present in the vadose zone, the trivalent elements readily sorb
503 to sediments, and their low solubility is thought to enhance partitioning to the solid phase, yielding large
504 K_D values and limiting migration (Krupka and Serne, 2002). Europium adsorption increases with
505 increasing pH and is nearly complete above pH 5 (Clark et al., 1998; Krupka and Serne, 2002). Under the
506 acidic pH range, the adsorption of europium is dominated by ion exchange and, therefore, decreases
507 with increasing ionic strength (Cantrell et al., 2007; Clark et al., 1998; Krupka and Serne, 2002;
508 Semenkova et al., 2023). However, when surface complexation reactions dominate europium sorption
509 (alkaline pH range) ionic strength has little impact and europium migration is limited even under
510 elevated ionic strength conditions (Krupka and Serne, 2002; Semenkova et al., 2023). Although the exact
511 pH in the vicinity of the sources is unknown, based on activity (Fig. S4 (a)) and pH measurements in the
512 effluent (Fig. S2), it is hypothesized that the elevated pH induced by the cementitious wastefoms
513 increased surface complexation to a greater extent than ion exchange was decreased by the enhanced
514 ionic strength. In these experiments, SRS sediments were observed to adsorb ^{152}Eu , limiting the overall
515 transport, and the incorporation of ^{152}Eu into a cementitious wastefom further limited migration. This is
516 corroborated by the consensus that europium sorbs strongly to cementitious materials (Wieland et al.,
517 2003). Furthermore, the cementitious materials served as physical barriers limiting the interaction
518 between ^{152}Eu and the surrounding environment. This aspect was enhanced in Reducing Grout-1 via the
519 incorporation of BFS and the subsequent reduction of the capillary pores (Matsuzuru et al., 1977). This is
520 consistent with the Reducing Grout-1 wastefom retaining the highest percentage of ^{152}Eu and exhibiting
521 the least migration.



522

(a)



523

(b)

524 Fig. 5. The distributions of ^{152}Eu activity as a function of distance from the approximate center of the
 525 source in (a) 2016 and (b) 2022. (PC-1 = Portland Cement-1, RG-1 = Reducing Grout-1, SC-1 = Sediment
 526 Control-1, SC-2 = Sediment Control-2, FWHM = full width at half maximum of the activity distribution in
 527 the lysimeter, FWQM = full width at quarter maximum of the activity distribution in the lysimeter). The
 528 plots illustrate the ^{152}Eu activity normalized by the decay corrected initial activity added to the system as
 529 a function of depth in the lysimeters. A depth of zero was assigned to the approximate center of the
 530 source. Note that only a 5 cm section is being shown of the 56 cm sediment column to demonstrate the
 531 differences between the lysimeters surrounding the source region. Note that the lines connecting the
 532 data points are simply for guidance

533

534

535 3.5. Radionuclide Activity Distribution Comparison

536 When the radionuclides were added directly to the sediment (Sediment Control-2), migration
537 increased in the order $^{152}\text{Eu} < ^{137}\text{Cs} < ^{60}\text{Co} < ^{133}\text{Ba}$, as shown by the lysimeter scans. Except for ^{137}Cs , the
538 downward transport of the radionuclides decreases with the increasing ionic potential. It is speculated
539 that hydroxy-interlayered vermiculate is present in the lysimeter sediment, providing highly selective
540 sites for ^{137}Cs , increasing sorption above what is expected based on ionic potential. Furthermore, under
541 the conditions typical of the SRS vadose zone, ^{60}Co and ^{133}Ba are highly soluble, and the SRS sediments
542 offer limited sorption sites for these radionuclides. The trend in the extent of radionuclide transport is
543 consistent with previously reported K_D values provided for SRS clayey sediments (Table S1). Based on the
544 width of the normalized activity distribution peaks, incorporation of the radionuclide suite into a
545 cementitious wastefrom resulted in the migration extent increasing in the order of
546 $^{152}\text{Eu} < ^{133}\text{Ba} < ^{60}\text{Co} < ^{137}\text{Cs}$. This order is consistent with the K_D values for the reducing grout, but based on
547 the K_D values for Portland Cement, the order of $^{152}\text{Eu} < ^{60}\text{Co} < ^{133}\text{Ba} < ^{137}\text{Cs}$ was anticipated. The percentage
548 of the radionuclides retained in the sources at the time of the 2022 measurements increased with the
549 cation charge. For Portland Cement-1, the percentage increased in the order $^{137}\text{Cs} < ^{60}\text{Co} \approx ^{133}\text{Ba} < ^{152}\text{Eu}$ and
550 for Reducing Grout-1 $^{137}\text{Cs} < ^{60}\text{Co} < ^{133}\text{Ba} < ^{152}\text{Eu}$. It is thought that although the percentages of ^{60}Co and
551 ^{133}Ba are similar in Portland Cement-1, the retention of ^{133}Ba is greater in Reducing Grout-1 due to the
552 tendency of this radionuclide to form insoluble precipitates with both sulfide and sulfate. In Portland
553 Cement-1, the migration of the radionuclides that leached into the sediment from the wastefrom was
554 reduced for all radionuclides except for ^{137}Cs , relative to the sediment control. The elevated ionic
555 strength in Portland Cement-1 is thought to have increased competition for cation exchange sites in the
556 sediment, limiting ^{137}Cs sorption (Fig. S3). However, Reducing Grout-1 limited the extent of migration
557 from the wastefrom edge for all radionuclides, including ^{137}Cs , due to reduced leaching and increased
558 sorption to the wastefrom.

559 4. Conclusions and Implications

560 Overall, the SRS-relevant K_D values accurately predicted the extent of migration for the suite of
561 radionuclides considered (Kaplan, 2021). The only exception to this is that in Portland Cement-1, the ^{60}Co
562 migration was expected to be less than that for ^{133}Ba due to the higher cobalt K_D value in oxidizing
563 cement. Compared to the sediment control, increased retention of the radionuclides in the sources was
564 observed in the lysimeters containing cementitious wastefroms. Furthermore, higher retention was
565 observed for Reducing Grout-1 than Portland Cement-1, particularly for ^{133}Ba and ^{137}Cs . However, in the
566 sediments surrounding the Portland Cement wastefrom, increased migration of ^{137}Cs was observed due
567 to competition with increased concentrations of competing cations. Reduced leaching and migration
568 through sediments was observed for all radionuclides in Reducing Grout-1.

569 These cementitious wastefroms act as a physical barrier that reduces the infiltration of water
570 and provides additional sorption sites for the radionuclides, slowing the initial radionuclide release into
571 the surrounding sediment. Relative to Portland cement, reducing grout has smaller capillary pores and
572 reduced hydraulic conductivity, limiting radionuclide leaching. Additionally, the sulfides and sulfates
573 present in reducing grout could have resulted in the precipitation or coprecipitation of some
574 radionuclides, limiting solubility and, thus, migration. The results of this study indicate that the Portland
575 cement did improve radionuclide retention relative to the sediment control, but it enhanced the
576 migration of ^{137}Cs which leached into the soil. Thus, the reducing grout was the superior material to

577 encapsulate the suite of radionuclides since it reduced migration and retained the highest percentage of
578 the radionuclides. Here, the migration of ^{60}Co , ^{133}Ba , ^{137}Cs , and ^{152}Eu at the Savannah River Site was
579 observed over a decade. However, this work demonstrates an effective method that can be reproduced
580 to determine site-specific values for other areas and radionuclides of interest.

581 **Declaration of competing interest**

582 The authors declare that they have no known competing financial interests or personal relationships that
583 could have appeared to influence the work reported in this paper.

584 **Declaration of Generative AI and AI-assisted technologies in the writing process**

585 During the preparation of this work the authors used Grammarly in order to check spelling and grammar.
586 After using this tool, the authors reviewed and edited the content as needed and take full responsibility
587 for the content of the publication.

588 **Data availability**

589 Data will be made available on request.

590 **Acknowledgments**

591 The operation and maintenance of the RadFLEx lysimeter test bed is supported in part by Savannah River
592 Mission Completion, LLC [Contract numbers SRRA175647 & SRRA2000036]. Analytical measurements
593 and data analysis was supported by the U.S. Department of Energy (US DOE) Office of Science, Office of
594 Basic Energy Sciences, Biological and Environmental Research program [Award Number DE-SC-0012530].
595 D. Kaplan acknowledges additional support from the US DOE, Office of Environmental Management
596 (Award Number DE-EM0005228) and US DOE Office of Environmental Management's Minority Serving
597 Institution Partnership Program (Task Order Agree #0000655879).

598 **Appendix A. Supporting information**

599 Supplementary data associated with this article can be found in the online version at doi: xxxxx

600 **References**

- 601 Aldahan, A., Haiping, Y., Possnert, G., 1999. Distribution of beryllium between solution and minerals
602 (biotite and albite) under atmospheric conditions and variable pH.
603 [https://doi.org/10.1016/S0009-2541\(98\)00186-7](https://doi.org/10.1016/S0009-2541(98)00186-7)
- 604 Almond, P., Kaplan, D., 2011. Distribution coefficients (KD) generated from a core sample collected from
605 the saltstone disposal facility (No. SRNL-STI-2010-00667, 1012546).
606 <https://doi.org/10.2172/1012546>
- 607 Andersson, K., Torstenfelt, B., Allard, B., 1983. Sorption and diffusion of Cs and I in concrete (No. SKBF-
608 KBS-TR--83-13). Chalmers University of Technology Göteborg, Sweden.
- 609 Arai, Y., Meena, A.H., Lenell, B., Powell, B.A., Kaplan, D.I., 2017a. Spatial distribution, chemical state,
610 solubility of rhenium in a reducing cement waste form: Implications for predicting technetium
611 mobility in saltstone. *Appl. Geochem.* 85, 180–187.
612 <https://doi.org/10.1016/j.apgeochem.2017.02.001>
- 613 Arai, Y., Powell, B.A., Kaplan, D.I., 2018. Residence time effects on technetium reduction in slag-based
614 cementitious materials. *J. Hazard. Mater.* 342, 510–518.
615 <https://doi.org/10.1016/j.jhazmat.2017.08.049>

- 616 Arai, Y., Powell, B.A., Kaplan, D.I., 2017b. Sulfur speciation in untreated and alkali treated ground-
617 granulated blast furnace slag. *Sci. Total Environ.* 589, 117–121.
618 <https://doi.org/10.1016/j.scitotenv.2017.02.163>
- 619 Bar-Nes, G., Peled, Y., Shamish, Z., Katz, A., 2017. Cesium and Strontium Immobilization in Portland
620 Cement Pastes Blended With Pozzolan Additives. *J. Nucl. Eng. Radiat. Sci.* 3, 030907.
621 <https://doi.org/10.1115/1.4035415>
- 622 Benjamin, M.M., 2015. *Water chemistry, Second Edition.* ed. Waveland Press, Inc., Long Grove, Illinois.
- 623 Brooks, S.C., Herman, J.S., Hornberger, G.M., Mills, A.L., 1998. Biodegradation of cobalt–citrate
624 complexes: Implications for cobalt mobility in groundwater. *J. Contam. Hydrol.* 32, 99–115.
625 [https://doi.org/10.1016/S0169-7722\(97\)00083-1](https://doi.org/10.1016/S0169-7722(97)00083-1)
- 626 Buesseler, K.O., Kaplan, D.I., Dai, M., Pike, S., 2009. Source-Dependent and Source-Independent Controls
627 on Plutonium Oxidation State and Colloid Associations in Groundwater. *Environ. Sci. Technol.* 43,
628 1322–1328. <https://doi.org/10.1021/es8028318>
- 629 Cantrell, K.J., Zachara, J.M., Dresel, P.E., Krupka, K.M., Serne, R.J., 2007. Geochemical Processes Data
630 Package for the Vadose Zone in the Single-Shell Tank Waste Management Areas at the Hanford
631 Site (No. PNNL-16663, 917584). <https://doi.org/10.2172/917584>
- 632 Chen, Q.Y., Tyrer, M., Hills, C.D., Yang, X.M., Carey, P., 2009. Immobilisation of heavy metal in cement-
633 based solidification/stabilisation: A review. *Waste Manag.* 29, 390–403.
634 <https://doi.org/10.1016/j.wasman.2008.01.019>
- 635 Clark, S.B., Bryce, A.L., Lueking, A.D., Gariboldi, J., Serkiz, S.M., 1998. Factors Affecting Trivalent f-Element
636 Adsorption to an Acidic Sandy Soil, in: *Adsorption of Metals by Geomedia.* Elsevier, pp. 149–164.
637 <https://doi.org/10.1016/B978-012384245-9/50006-2>
- 638 Dixon, Joe Boris, Weed, Sterling Barg, Dixon, Joe B., Weed, S. B., Soil Science Society of America (Eds.),
639 1989. *Minerals in soil environments, 2. ed., reprint.* ed, Soil Science Society of America book
640 series. Soil Science Society of America, Madison, Wis.
- 641 Dragun, J., 1988. *The soil chemistry of hazardous materials.* Hazardous Materials Control Research
642 Institute, Silver Spring, Md.
- 643 Erdmann, B.J., Powell, B.A., Kaplan, D.I., DeVol, T.A., 2018. One-dimensional Spatial Distributions of
644 Gamma-ray Emitting Contaminants in Field Lysimeters Using a Collimated Gamma-ray
645 Spectroscopy System. *Health Phys.* 114, 532–536.
646 <https://doi.org/10.1097/HP.0000000000000799>
- 647 Estes, S.L., Arai, Y., Becker, U., Fernando, S., Yuan, K., Ewing, R.C., Zhang, J., Shibata, T., Powell, B.A., 2013.
648 A self-consistent model describing the thermodynamics of Eu(III) adsorption onto hematite.
649 *Geochim. Cosmochim. Acta* 122, 430–447. <https://doi.org/10.1016/j.gca.2013.08.023>
- 650 Eylem, C., Erten, H.N., Göktürk, H., 1990. Sorption-desorption behaviour of barium on clays. *J. Environ.*
651 *Radioact.* 11, 183–200. [https://doi.org/10.1016/0265-931X\(90\)90061-Y](https://doi.org/10.1016/0265-931X(90)90061-Y)
- 652 Giannakopoulou, F., Haidouti, C., Chronopoulou, A., Gasparatos, D., 2007. Sorption behavior of cesium
653 on various soils under different pH levels. *J. Hazard. Mater.* 149, 553–556.
654 <https://doi.org/10.1016/j.jhazmat.2007.06.109>
- 655 Gilliam, T.M., Spence, R.D., Bostick, W.D., Shoemaker, J.L., 1990. Solidification/stabilization of technetium
656 in cement-based grouts. *J. Hazard. Mater.* 24, 189–197. [https://doi.org/10.1016/0304-3894\(90\)87009-7](https://doi.org/10.1016/0304-3894(90)87009-7)
- 657
- 658 Goñi, S., Guerrero, A., Lorenzo, M.P., 2006. Efficiency of fly ash belite cement and zeolite matrices for
659 immobilizing cesium. *J. Hazard. Mater.* 137, 1608–1617.
660 <https://doi.org/10.1016/j.jhazmat.2006.04.059>
- 661 Goo, J.-Y., Kim, B.-J., Kang, M., Jeong, J., Jo, H.Y., Kwon, J.-S., 2021. Leaching Behavior of Cesium,
662 Strontium, Cobalt, and Europium from Immobilized Cement Matrix. *Appl. Sci.* 11, 8418.
663 <https://doi.org/10.3390/app11188418>

- 664 Goto, M., Rosson, R., Elliott, W.C., Wampler, J.M., Serkiz, S., Kahn, B., 2014. Interactions of radioactive
665 and stable cesium with hydroxy-interlayered vermiculite grains in soils of the Savannah River
666 Site, South Carolina, USA. *Clays Clay Miner.* 62, 161–173.
667 <https://doi.org/10.1346/CCMN.2014.0620301>
- 668 Goto, M., Rosson, R., Wampler, J.M., Elliott, W.C., Serkiz, S., Kahn, B., 2008. Freundlich and dual Langmuir
669 isotherm models for predicting ¹³⁷Cs binding on Savannah River Site soils. *Health Phys.* 94, 18–
670 32. <https://doi.org/10.1097/01.HP.0000278416.04381.31>
- 671 Hinton, T.G., Kaplan, D.I., Knox, A.S., Coughlin, D.P., Nascimento, R.V., Watson, S.I., Fletcher, D.E., Koo, B.-
672 J., 2006. Use of Illite Clay for In Situ Remediation of ¹³⁷Cs-Contaminated Water Bodies: Field
673 Demonstration of Reduced Biological Uptake. *Environ. Sci. Technol.* 40, 4500–4505.
674 <https://doi.org/10.1021/es060124x>
- 675 Jeong, C., Cho, Y., Hahn, P., 1998. Influence of Ionic Strength, pH, and Complex-forming Anions on the
676 Adsorption of Cesium-137 and Strontium-90 by Kaolinite. *Korean Soc. Econ. Environ. Geol.* 31,
677 11–20.
- 678 Kaplan, D.I., 2021. Geochemical data package for performance assessment calculations related to the
679 Savannah River Site (No. SRNL-STI--2021-00017, 1772357). <https://doi.org/10.2172/1772357>
- 680 Kaplan, D.I., Powell, B., Barber, K., Devol, T., Dixon, K., Erdmann, B., Maloubier, M., Martinez, N.,
681 Montgomery, D., Peruski, K., Roberts, K., Witmer, M., 2017. Radionuclide field lysimeter
682 experiment (RadFLEX): geochemical and hydrological data for SRS performance assessments (No.
683 SRNL--STI-2017-00677, 1418133). <https://doi.org/10.2172/1418133>
- 684 Kaplan, D.I., Roberts, K., Coates, J., Siegfried, M., Serkiz, S., 2008. Saltstone and concrete interactions
685 with radionuclides: sorption (KD), desorption, and reduction capacity measurements.
686 <https://doi.org/10.2172/944861>
- 687 Kaplan, D.I., Serkiz, S.M., Allison, J.D., 2010. Europium sorption to sediments in the presence of natural
688 organic matter: A laboratory and modeling study. *Appl. Geochem.* 25, 224–232.
689 <https://doi.org/10.1016/j.apgeochem.2009.11.007>
- 690 Kim, J.H., Gibb, H.J., Howe, P.D., World Health Organization. Chemical Safety Team, International
691 Programme on Chemical Safety, 2006. Cobalt and inorganic cobalt compounds / prepared by
692 James H. Kim, Herman J. Gibb, Paul D. Howe. Concise international chemical assessment
693 document ; 69.
- 694 King, L.D., 1988. Retention of Metals by Several Soils of the Southeastern United States. *J. Environ. Qual.*
695 17, 239–246. <https://doi.org/10.2134/jeq1988.00472425001700020013x>
- 696 Komljenović, M., Tanasijević, G., Džunuzović, N., Provis, J.L., 2020. Immobilization of cesium with alkali-
697 activated blast furnace slag. *J. Hazard. Mater.* 388, 121765.
698 <https://doi.org/10.1016/j.jhazmat.2019.121765>
- 699 Krupka, K.M., Serne, R.J., 2002. Geochemical Factors Affecting the Behavior of Antimony, Cobalt,
700 Europium, Technetium, and Uranium in Vadose Zone Sediments (No. PNNL-14126, 15004491).
701 <https://doi.org/10.2172/15004491>
- 702 Kumar, A., Komarneni, S., Roy, D.M., 1987. Diffusion of Cs⁺ and Cl⁻ through sealing materials. *Cem.*
703 *Concr. Res.* 17, 153–160. [https://doi.org/10.1016/0008-8846\(87\)90069-X](https://doi.org/10.1016/0008-8846(87)90069-X)
- 704 Landry, C.J., Koretsky, C.M., Lund, T.J., Schaller, M., Das, S., 2009. Surface complexation modeling of Co(II)
705 adsorption on mixtures of hydrous ferric oxide, quartz and kaolinite. *Geochim. Cosmochim. Acta*
706 73, 3723–3737. <https://doi.org/10.1016/j.gca.2009.03.028>
- 707 Langmuir, D., 1997. Aqueous environmental geochemistry. Prentice Hall, Upper Saddle River, N.J.
- 708 Li, K., Pang, X., 2014. Sorption of radionuclides by cement-based barrier materials. *Cem. Concr. Res.* 65,
709 52–57. <https://doi.org/10.1016/j.cemconres.2014.07.013>

- 710 Matsuzuru, H., Moriyama, N., Wadachi, Y., Ito, A., 1977. Leaching Behavior of Cesium-137 in Cement-
711 waste Composites: *Health Phys.* 32, 529–534. [https://doi.org/10.1097/00004032-197706000-](https://doi.org/10.1097/00004032-197706000-00008)
712 00008
- 713 McLaren, R.G., Lawson, D.M., Swift, S., 1986. The forms of cobalt in some Scottish soils as determined by
714 extraction and isotopic exchange. *J. Soil Sci.* 37, 223–234. [https://doi.org/10.1111/j.1365-](https://doi.org/10.1111/j.1365-2389.1986.tb00023.x)
715 2389.1986.tb00023.x
- 716 Mendez, J.C., Hiemstra, T., 2020. Surface area of ferrihydrite consistently related to primary surface
717 charge, ion pair formation, and specific ion adsorption. *Chem. Geol.* 532, 119304.
718 <https://doi.org/10.1016/j.chemgeo.2019.119304>
- 719 Mitchell, J.K., Soga, K., 2005. *Fundamentals of soil behavior*, 3. ed. ed. Wiley, Hoboken, NJ.
- 720 Montgomery, D., Barber, K., Edayilam, N., Oqujiuba, K., Young, S., Biotidara, T., Gathers, A., Danjaji, M.,
721 Tharayil, N., Martinez, N., Powell, B., 2017. The influence of citrate and oxalate on 99TcVII, Cs,
722 NpV and UVI sorption to a Savannah River Site soil. *J. Environ. Radioact.* 172, 130–142.
723 <https://doi.org/10.1016/j.jenvrad.2017.03.017>
- 724 Narendrula, R., Nkongolo, K.K., Beckett, P., 2012. Comparative Soil Metal Analyses in Sudbury (Ontario,
725 Canada) and Lubumbashi (Katanga, DR-Congo). *Bull. Environ. Contam. Toxicol.* 88, 187–192.
726 <https://doi.org/10.1007/s00128-011-0485-7>
- 727 Naumann, T.E., Elliott, W.C., Wampler, J.M., 2012. K-Ar Age Constraints on the Origin of Micaceous
728 Minerals in Savannah River Site Soils, South Carolina, USA. *Clays Clay Miner.* 60, 496–506.
729 <https://doi.org/10.1346/CCMN.2012.0600506>
- 730 Naveau, A., Monteil-Rivera, F., Dumonceau, J., Boudesocque, S., 2005. Sorption of europium on a
731 goethite surface: influence of background electrolyte. *J. Contam. Hydrol.* 77, 1–16.
732 <https://doi.org/10.1016/j.jconhyd.2004.10.002>
- 733 Ochs, M., Mallants, D., Wang, L., 2016. Radionuclide and metal sorption on cement and concrete, Topics
734 in safety, risk, reliability and quality. Springer, Cham Heidelberg New York.
- 735 Payne, T.E., Itakura, T., Comarmond, M.J., Harrison, J.J., 2009. Environmental mobility of cobalt—
736 Influence of solid phase characteristics and groundwater chemistry. *Appl. Radiat. Isot.* 67, 1269–
737 1276. <https://doi.org/10.1016/j.apradiso.2009.02.026>
- 738 Peruski, K., Pope, R., Maloubier, M., Powell, B.A., 2017. Determination of constituent concentrations in
739 field lysimeter effluents (No. SRRA021685- 000008). Clemson University, Anderson, SC.
- 740 Powell, B.A., Arai, Y., 2015. Examination of Tc, S, and Fe speciation within saltstone (No. SRRA042328).
741 Clemson University, Anderson, SC.
- 742 Roberts, K., Kaplan, D., Bagwell, L., Powell, B., Almond, P., Emerson, H., Hixon, A., Jablonski, J., Buchanan,
743 C., Waterhouse, T., 2012. SRNL radionuclide field lysimeter experiment: baseline construction
744 and implementation (No. SRNL-STI-2012-00603, 1053691). <https://doi.org/10.2172/1053691>
- 745 Santikari, V.P., Witmer, M., Murdoch, L.C., Kaplan, D.I., Powell, B.A., 2022. Leaching and transport of
746 technetium from reducing cementitious waste forms in field lysimeters. *Sci. Total Environ.* 841,
747 156596. <https://doi.org/10.1016/j.scitotenv.2022.156596>
- 748 Seaman, J., Chang, H., 2013. Impact of Cementitious Material Leachate on Contaminant Partitioning (No.
749 R-13-0004, Ver. 1.0). Savannah River Ecology Laboratory, Aiken, SC.
- 750 Semenkov, A.S., Romanchuk, A.Yu., Seregina, I.F., Mikheev, I., Svitelman, V.S., Kalmykov, S.N., 2023.
751 Eu(III) sorption on kaolinite: Experiments and modeling. *Appl. Clay Sci.* 234, 106865.
752 <https://doi.org/10.1016/j.clay.2023.106865>
- 753 Spark, K.M., Wells, J.D., Johnson, B.B., 1995. Characterizing trace metal adsorption on kaolinite. *Eur. J.*
754 *Soil Sci.* 46, 633–640. <https://doi.org/10.1111/j.1365-2389.1995.tb01359.x>
- 755 Sposito, G., 1989. *The chemistry of soils*. Oxford Univ. Pr, New York, NY.

- 756 Tits, J., Stumpf, T., Rabung, T., Wieland, E., Fanghänel, T., 2003. Uptake of Cm(III) and Eu(III) by Calcium
757 Silicate Hydrates: A Solution Chemistry and Time-Resolved Laser Fluorescence Spectroscopy
758 Study. *Environ. Sci. Technol.* 37, 3568–3573. <https://doi.org/10.1021/es030020b>
- 759 Wieland, E., Bradbury, M.H., Van Loon, L., 2003. Development of a sorption data base for the
760 cementitious near-field of a repository for radioactive waste. *Czechoslov. J. Phys.* 53, A629–A638.
761 <https://doi.org/10.1007/s10582-003-0081-0>
- 762 Woodward, G.L., Peacock, C.L., Otero-Fariña, A., Thompson, O.R., Brown, A.P., Burke, I.T., 2018. A
763 universal uptake mechanism for cobalt(II) on soil constituents: Ferrihydrite, kaolinite, humic acid,
764 and organo-mineral composites. *Geochim. Cosmochim. Acta* 238, 270–291.
765 <https://doi.org/10.1016/j.gca.2018.06.035>
- 766 Zaunbrecher, L.K., Elliott, W.C., Wampler, J.M., Perdrial, N., Kaplan, D.I., 2015. Enrichment of Cesium and
767 Rubidium in Weathered Micaceous Materials at the Savannah River Site, South Carolina. *Environ.*
768 *Sci. Technol.* 49, 4226–4234. <https://doi.org/10.1021/es5054682>
- 769